Max-Planck-Institut für Meteorologie

REPORT No. 13

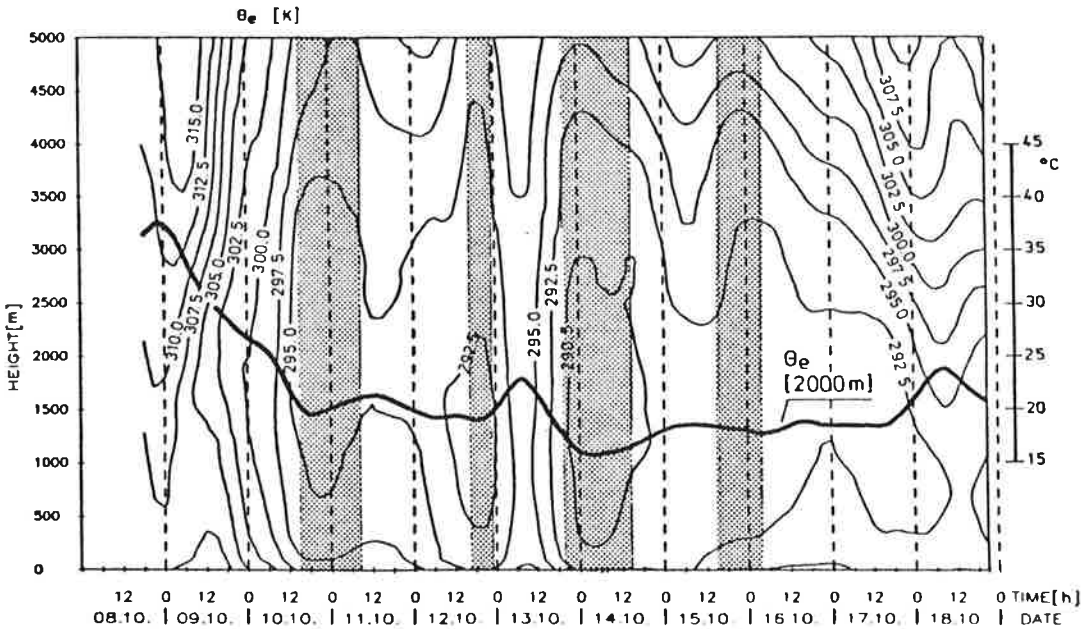

THE ATMOSPHERIC STRUCTURE IN OPEN CELLULAR CONDITIONS DURING KONTUR 1981

by

GOTTFRIED KRUSPE · STEPHAN BAKAN

HAMBURG, FEBRUARY 1988

AUTHORS:

GOTTFRIED KRUSPE — MAX-PLANCK-INSTITUT FÜR METEOROLOGIE

STEPHAN BAKAN — MAX-PLANCK-INSTITUT FÜR METEOROLOGIE

MAX-PLANCK-INSTITUT
FÜR METEOROLOGIE
BUNDESSTRASSE 55
D-2000 HAMBURG 13
F.R. GERMANY

Telefon nat.: (040) 41 14 - 1
Telefon int.: + 49 40 41 14 - 1
Telex-Nr.: 211092
Telemail: MPI.METEOROLOGY
Telefax nat.: (040) 41 14 - 298
Telefax int.: + 49 40 41 14 - 298

The atmospheric structure in open cellular conditions during KonTur 1981

G. Kruspe and S. Bakan
Max-Planck-Institut für Meteorologie
Hamburg, FRG

Abstract

The KonTur 1981 experiment was primarily dedicated to the study of organized boundary layer convection. While two research aircraft were available for detailed boundary layer measurements an aerological network of four stations in the German Bight (North Sea) yielded the information on the larger scale atmospheric structure in organized convective situations.

During the second experiment phase in October 1981 cold air advection caused intense convective activity. Four periods of well organized open convection cells could be determined from NOAA satellite images. The present paper contains the results from the aerological data set.

Cellular episodes appeared during rather cold and dry periods in which equivalent potential temperature reached a minimum. Nevertheless, the mean atmospheric profiles do not differ considerably from those found under convective conditions without cellular organization. In addition the aerological network allowed to derive horizontal gradients with acceptable accuracy. These show generally small values near the accuracy limits throughout the convection layer during the cellular episodes. On the other hand significant values are found during cold air advection before and warm air advection after these phases. Finally, the evolution of the best expressed cellular episode is presented in a case study.

1. *Introduction*

Cold air advection over sea is frequently accompanied by the organisation of convective clouds into fairly regular structures (Fig. 1a). These are characterized by more or less ringlike cloud groups with a typical diameter of 30 to 50 km. It is believed, that the cloudy walls mark areas of average lifting of air due to a convectively driven secondary circulation, while the cloudfree interior is due to compensating subsidence (Fig. 1b).

Since the advent of meteorological observation satellites this phenomenon has been repeatedly described and documented (e.g. Krueger and Fritz, 1961; Agee et al., 1973). The derivation of quantitative data in organized open cellular situations, however, turned out to be a difficult task. This is due to the mesoscale nature of the phenomenon that occurs almost exlusively over the ocean. Satellite images yield information on the horizontal planform but cannot tell too much about the vertical structure.

Therefore, several studies on the structure of the large scale field have been carried through. But except for several estimations of the aspect ratio (diameter / depth) no information about the cellular structure itself has been published.

From a statistical analysis of 106 cases of open cellular convection near Weather-ship M (~ 65°N, 2°E) typical surface conditions were derived (Busack et al., 1985). On the average the air-sea temperature difference was -4.7 ± 2.4°C and the wind speed 11.1 ± 4.8 m/s. Sensible and latent heat fluxes reached 89 ± 55 and 138 ± 65 W/m^2, respectively, corresponding to a rather high Bowen-ratio of 0.64. The average horizontal divergence turned out to be very small ($1.2 \cdot 10^{-6}$ s^{-1}).

Krueger and Fritz (1961) evaluated several radio soundings from routine stations in the subtropics when the satellite image showed open cellular convection. They found an adiabatically stratified layer of moist air about 1500 m deep, heated from the ocean, which was capped by a layer of greater stability. Throughout the convective layer there appeared to be little variation in wind speed and direction above the surface friction. Furthermore, they noted a typical diameter to depth ratio of about 30, as opposed to values of 2 to 3 for laboratory convection. This discrepancy is not yet really understood, although various tentative explanation have been put forward.

During AMTEX 1974/75 an experimental study of organized convection in cold air outbreaks was possible for the first time (Lenschow and Agee, 1976). Sheu and Agee (1977) report that the observed cases of open convection cells were associated with

- large scale divergence and sinking
- sea-air temperature differences larger than 5 K
- surface wind speeds above 5 m/s.

During September/October 1981 the experiment KonTur (Hinzpeter, 1985) took place over the German Bight with the main goal of studying convection and turbulence in the marine boundary layer. Special emphasis was put on the observation of organized boundary layer roll and cellular convection. On several occasions during the experiment boundary layer rolls have been observed (Brümmer, 1985), spurring a number of theoretical studies of the phenomenon (Chlond, 1985, Shirer, 1986, Shirer and Brümmer, 1986, Chlond, 1987, Becker, 1987).

During the second phase of the experiment a 4 day period of cold air advection into the North Sea allowed to study open cellular convection rather thoroughly by a network of surface and radiosonde stations and by two research aircraft. The surface and radiosonde network was planned to yield the mean large scale conditions during convective situations, while the aircraft could also study properties of single cells. Results of surface and airplane observations have been published already (Bakan, 1985; Brümmer et al., 1986), together with a first modelling attempt (Beniston, 1984, 1985). As a support for similar studies and as an interesting additional information in its own right the aerological findings of this second KonTur phase are supplemented in the present paper.

2. The observations

KonTur 1981 was the first and, hitherto, only experiment, that allowed the study of open cellular convection over the ocean in detail.

The experimental setting has been described in detail in the field phase report (Hoeber, 1982). The primary purpose of the radiosonde program was to observe continuously throughout the experiment the mean large-scale thermodynamic and kinematic quantities.

The aerological program consisted of four stations with a sounding schedule that frequently enclosed periods with only 90 minutes distance between coordinated launches. The following four ship-stations formed the KonTur aerological network in the German Bight (Fig. 2): BORKUM RIFF (58.8N, 6.4E), POSEIDON (55.2 N, 6.1 E), METEOR (55.0 N, 7.9 E), and ELBE 1 (54.0 N, 8.1 E).

The appearence of the convection cells and their state of organization were derived from NOAA-satellite images, which were available every 6 hours. The period of best organization occurred from the evening Oct. 13 until the morning of Oct. 14.

2.1. Aerological measurements

At the ship stations (except for the RV METEOR) Vaisala aerological set-ups of the FGGE-type were deployed. These were to a certain extent black boxes, providing no real-time data read-out. At the RV METEOR, the aerological equipment was a Vaisala MicroCora system, which proved to be very useful for control purposes and quick look. Vaisala-radiosondes of the Type RS20 were used, which transmit frequency modulated signals at a carrier frequency between 395 and 410 MHz. The 100g-ballons were filled with 0.6 cbm Helium to provide an ascent rate of about 300 m/min. Pressure, temperature, relative humidity, wind speed and wind direction were output every 10 seconds on cassetts.

Winds were obtained by Navaid wind finding, which provides the wind by reference to the global radionavigation aid system. The resulting wind velocities should be accurate to within 2.0 m/s. That is due to generally good signal-strengths from at least three stations. Additional smoothing of the OMEGA-phases over 2 minutes on either side of the designated time turned out to be necessary for acceptable wind quality. Therefore, reliable wind-data are available only for heights above roughly 500 m.

Rms-accuracies of the thermodynamic quantities after correction of the radiation influence on the thermistor and of the self-heating effect of the humicap are about 1 hPa for pressure (aneroid cell), 0.3 K for temperature (thermistor), and 8% for relative humidity (Humicap hygrometer).

The launching-schedule during the period in consideration varied from 4 to 8 soundings per day (Fig. 3). However, during periods of strong winds it turned out

to be extremely difficult to keep up with the planned schedule, due to problems with the balloon handling. Therefore, the data volume is less than originally planned. Table 1 lists the amount of complete soundings and failures as well as the number of simultaneous starts accomplished for both KonTur field phases. Nevertheless, the resultant aerological data set should yield reliable horizontal averages as well as gradients of various quantities down to periods around 6 hours.

2.2. Data quality control

Primary processing of the aerological data was done by using the Vaisala editing software of the MicroCora, which eliminates noise from the data, and checks that vertical changes of the various parameters are within acceptable limits. In addition, obviously bad data are removed by manual intervention. Geopotential heights were recalculated after offset correction of the surface pressure data which are calculated with the North Sea objective analysis scheme of Luthart (1987) from the GTS network data. The data-sets were also tested for horizontal and temporal consistency. Horizontal gradients of pressure, temperature, humidity, and wind were calculated by least square fit methods, assuming a first-order plane. Temporal tendencies were determined by detecting both, preceding and subsequent observations from the same stations.

The data were interpolated to 50 m height-intervalls. Deriving mean meteorological fields, and minimizing local and subgrid variations, time series with hourly steps were created by interpolation of neighbouring soundings for each particular height. These data were smoothed by a cosine-taper over 4 hours on either side of the designated times and sampled in steps of 3 hours. For vertical smoothing, a Hanning-taper was used.

3. Synoptic conditions

The dominating synoptic features over the North Sea during the second phase of the KonTur experiment (Fig. 4) can be classified as

a. cyclonic westregime (from 9-12 October), maritime polar air mass,
b. cyclonic NW-regime (13 October), martime arctic air mass,
c. an anticyclonic westregime (14-17 October), maritime arctic air mass.

From the waved, but mainly zonally aligned polar frontal-zone near 60N, that slowly moved southwards, an intensive synoptic activity was initiated especially

from Oct. 9 to Oct. 14. This period is characterized by instationary conditions in which several front-systems travelled eastwards along that waved frontal zone over the North Sea to Scandinavia. The resulting nearly periodical cold air outbreaks replaced the initially polar maritime air mass by arctic maritime air, when the synoptic situation changed from cyclonic west to northwest. Due to the intensive synoptic activity periods of quasi-stationary conditions in the KonTrol area of more than 20 hours did not occur.

Cold air pushes are followed by phases of relatively dry and stable air in which these convective cell pattern of different regularity were observed as intermediate states.

4. Results

4.1. Time development at the surface

The time development of horizontally averaged surface data at 10 m height and of derived quantities (Fig. 5) represent the situation, during which four pronounced episodes of cellular events were observed. Remarkable foot prints of well expressed cellular events are not obvious in any of these time series. In agreement with other observations, the following conditions were observed: The temperature of the water surface (Tw) exceeded the air temperature (Ta) by more then 3 K, and relative humidity (RH) was rather small ($< = 70\%$). The inflow of relatively cool and dry polar air stimulated unstable stratification ($-z/L \approx 0.3$), and rather large turbulent fluxes of sensible ($H > 80$ W/m^2) and latent heat (l E > 200 W/m^2). As indicated by the Bowen ratio, latent heat fluxes were roughly 2.5 times larger than sensible heat fluxes. The lifting condensation level as derived from data at 10 m height, was found between.5 and .8 km height during the different cellular phases.

4.2. Time development of mean fields

The time cross section of various quantities as shown in Figs. 6-10 have been produced from spacial averages of the soundings of at least two aerological stations smoothed with respect to time. Many synoptic details may be recognized in the figures, which are of interest to the study of cellular events (hatched areas).

4.2.1. Thermodynamic quantities

Potential temperature (Fig. 6)

Potential temperature may intuitively be believed to correlate best of all to the appearence of open cells. Indeed, the potential temperature isolines reach maximum heights during the convective situations due to advection of cold air.

Four phases of cold air pushes can be localized, which are separated from warming phases by imbedded quasi stationary isentropic minima of different time extension. These phases were found to be quite in coincidence with well expressed cellular organization. This was especially striking for the third phase of about 20 hours duration. Obviously, anticipating here later results, this indicates, that well expressed cellular convective structures may preferably exist in pools of rather stationary and horizontally homogeneous cold air.

Specific and relativ humidity (Figs. 7, 8)

The moisture field clearly reflects the synoptic situation. In reference to the four defined phases of cold air invasion, cooling before the onset of cellular pattern is strongly correlated with drastically drying phases, as can be drawn from the steeply declining isolines of specific humidity in Fig. 7. The local minima of these isolines coincide with the above mentioned cold air pools, in which cellular convection is best developed.

In contrast to specific humidity, the relative humidity field in Fig. 8 does not exhibit a very obvious relation to the cellular periods. Nevertheless, the time course of the 60% isoline represents at least qualitatively the evolution of the convective boundary layer, which generally is topped by a stable and relatively dry midtropospheric advection layer. The first phase (until Oct. 12) of predominantly cyclonic cold air invasion is characterized by growth of the convective boundary layer from about 2 km to 4 km. The day after deep convection prevailed, so that up to 5 km height relative humidity of more than 60% was found. The forced anticyclonic influence, which set in on the evening of Oct. 13, led to the successive decline of the respective isoline with a rate of -1.1 km/day which led to the end of the cellular episode.

Equivalent potential temperature (Fig. 9)

Equipotential temperature is widely considered to be useful for air mass identification. In the preceding section, both potential temperature and specific humidity were found to exhibit a relative minimum during the occurrence of well expressed cellular convection. Consequently, the mean field of equipotential temperature distinguishes those periods clearly by showing a well expressed minimum. The closed isolines indicate an environment of quite stationary and horizontally homogeneous conditions. Also the vertical variations are rather small within the convection layer.

The first and the third of these cellular events appeared after active cold frontal events, which are represented by a dense local pattern of nearly vertically aligned isolines. Thereby, the depth of the convective layer is increased up to more than 5 km. The other two cases follow passive cold air invasions after intermediate phases of slight warming.

The end of the cellular phases is marked by an equivalent potential temperature increase due to moist and warm air advection in subsident flow at the west side of transient ridges.

4.2.2. Dynamic quantities

While thermodynamic quantities exhibit characteristic common features during the cellular stages, neither wind speed (Fig. 10), nor direction, nor the kinematic quantities as divergence and relative vorticity (as will be shown in ch. 4.2) do so.

During well expressed cellular phases, as well as during most of the second KonTur-period, the vertical variation of wind speed in the convection layer is small. Those active cold frontal events preceeding the cellular phases 1 and 3 were coupled with high wind speeds which are rapidly decreasing during the cellular phases. On the other hand wind speed does not change considerably during cellular phases 2 and 4 and does not differ significantly from the wind speed before or after the events.

4.3. Time development of horizontal gradients

Time series of the mean horizontal vector fields of pressure, temperature, and specific humidity gradients, as well as of horizontal divergence are given in Figs. 11-13, and 15. The vector fields are symbolized by arrows, which point in the direction of the steepest decrease of the particular quantity. Their lengths represent the value of the gradient in that particular direction. According to the measurement accuracies of single stations (compare. ch 2.2), the RMS errors of the horizontal gradients should be less than 5. hPa/1000 km for pressure, 3K/1000 km for temperature, 3g/kg/1000 km for specific humidity, and 10^{-5}/sec for wind speed gradients. Additional uncertainty may be introduced in a convective situation by unpredictable and unrecoverable flight radiosonde paths in the vicinity of clouds. Therefore, different history of simultaneously launched sondes may lead to apparent gradients.

Pressure gradient field (Fig. 11): The dominating feature of the synoptic weather situation as described in ch. 3.1 is clearly reflected by the pressure gradient field. The eastward movement of the gale type cyclonic depression north of the KonTur area from the beginning of the second KonTur phase (situated near Ireland on Oct. 9 and over the Norwegian Sea on Oct. 15) is documented by the directional change of the arrows. Strongest pressure gradients, which exceed 40 hPa/1000 km in the KonTur area, occurred on Oct. 10/11 as well as on Oct. 13, where a small depression center, coupled with trough development suddenly originated in the North Sea. Riehl (1982) analyzed the thermal structure of this "warm low and trough" as a medium scale high energy center, which passed the area between 6.00 and 12.00 UT (compare also temperature gradient field in Fig. 14).

Due to intensive synoptic activity, horizontal pressure force is varying with time which is closely tied to the evolution of the wind field (compare Fig. 12). Periods of organized convection show vertically rather constant pressure gradients which, generally, implies small vertical change of geostrophic (thermal) wind. Accordingly the observed wind shows only minor vertical changes (ch. 4.2.2).

Temperature gradient field and temperature advection (Figs. 12-13): The time course of the temperature gradient vector field clearly reflects the passage of cold frontal events preceding the cellular periods. Obviously, the cellular phases (except for the second one) were characterized by reduced baroclinicity in the

convection layer. Another conspicuous feature of the baroclinitity field is the larger directional difference of the baroclinicity between the lower (< 2000 m) and the middle troposphere especially on Oct. 10/11 and 14. This may indicate the modification of the synoptic baroclinicity field by shallow, medium scaled disturbances and/or by spacially different latent heating.

Temperature advection (Fig. 13) is quite remarkable during the periods, that preceed, respectively, succed the cellular stages. On the other hand small values are found in the convective layer during the cellular periods.

Moisture gradient field (Fig. 14): With respect to the cellular phases the moisture gradient field does not exhibit striking common features. The gradients are generally found to be small, except for heights between 1.5 and 3.5 km during the first active cold frontal event on October 10 where values of 30 g/kg/1000 km are reached. At the same time the horizontal moisture advection resulted in drying rates > 10 g/kg/day, but does not significantly exceed the accuracy limits during the remaining time.

Divergence (Fig. 15) and relative vorticity: From the wind data horizontal wind gradients and resulting divergence and vorticity were determined. Except for frontal events divergences are in general near the accuracy limits. The remaining divergence pattern does not show a strong correlation with the cellular periods. Nevertheless, Fig. 15 indicates that during cellular periods the flow in the lower troposphere tended to be convergent.

Augstein (1982), derived from a simplified analysis of unvalidated wind data below cloud base convergence values of $3 \cdot 10^{-5}\,s^{-1}$. As a consequence, the author suggested that the related large scale convergence of moisture and heat flux below cloud base may be of greater importance for moist convective processes during cellular events than surface fluxes.

On the other hand Luthardt (1985) found from surface data no significant sign of the surface divergence over the open sea but some indication of coastal convergence. As two of the KonTur platforms BORKUM RIFF and ELBE 1 are only around 30 km off shore the superposition of coastal convergence has to be considered.

The time cross section of relative vorticity, too, does not show significant values during the cellular periods.

4.4. Vertical profiles during a well expressed cellular phase

In this chapter the typical evolution of a cellular episode is documented by data from the best developed period 3 as a case study. Therefore, the mean vertical structure of several thermodynamic and dynamic quantities during the preceding (phase A: Oct. 13, 900-1800 UT), cellular (phase B: Oct. 14, 900-1800 UT) and succeeding (phase C: Oct. 14, 2100 - Oct. 15, 600 UT) development stages are presented (Fig. 16).

The vertical profiles of potential temperature are rather similar in all three phases below cloud base. In the cloud layer the stability was found to be reduced during the organized convective phase B as compared to the other phases. Above 4000 m a progressive stabilization was observed.

The boundary layer was found during three phases A-C to be conditionally unstably stratified all up to 1.5 km height. Also the lifting condensation level does not show any striking difference.

The profiles of Θe are quite similar during phases A and B up to 4 km height above which during the cellular stage a more stable state, prevails. This clearly corresponds to the humidity profiles, which show in phase A secondary maxima, that fairly mark levels of deeper convective clouds. In the cellular phase B, the mean cloud top is around 3 km height. Phase C represents the progress of further stabilization and penetration of dry air into lower levels.

As is typical of open cellular conditions, the wind profile below 3 km height is rather constant without any striking difference in the vertical profiles during all phases. Above that height increasing wind shear occurs together with increasing stability during phases B and C.

In Table 2, surface data as well as tendency and advection terms are listed for several heights for all three phases A-C. Phase A and B are characterized by large turbulent surface heat fluxes, which decreased during phase C due to the reduced surface wind speed.

Tendencies of temperature were quite remarkable during phase A (vertically increasing cooling) and C (vertically increasing warming), but insignificant up to 3 km height during the appearence of organized convection cells. With respect to pressure, there is a pronounced increase only during phase A (inflow of denser cold air). Wind tendencies are generally psoitive in phase A and negative during phases B and C.

Thermal advection (-v * grad T) values show strong cooling in phase A and remarkable warming during phase C, but hardly any heating during the cellular phase B. The result underlines the important role of large scale advection in the middle troposphere on the convective evolution.

One problem of interpretation of convection data becomes obvious from these profiles: Which of the possible layer depth definitions would yield a convection height, that could be compared to such heights used in theoretical modelling. In model studies usually a rigid upper lid confines the convection layer to a well defined depth. In the atmosphere potential temperature does not show any well defined inversion above the convection layer. Therefore, this profile is hard to use for such a height definition. The relative humidity profile on the other hand seems to give a rather clear reduction above the clouds. But the possible height deduced from this profile may vary between 2500 and 4000 m. This issue cannot be solved from our data, but they indicate that great care has to be taken if the derivation of such a convective height is desired.

5. Conclusions

During the second phase of KonTur 1981 cold air advection led to intense convective activity in the experimental area with embedded events of well organized cellular convection. The picture that emerges from the observed time series is as follows: Embedded in a cold air flow were various "pools" of even colder air showing up in the satellite images as areas with especially well developed open cellular structure. These areas are characterized by small vertical gradients of wind speed and direction, of equivalent potential temperature, and by small horizontal gradients of thermodynamic quantities indicating strong vertical and horizontal mixture due to convective activity. These cold pools represent smaller values of equivalent potential energy than prevail in the surrounding parts of the flow.

Several problems with the evaluation of measurements have to be noted:
First of all the method of defining well organized cellular episodes from satellite images is subjective, as their existence has been decided by eye inspection of 6-hourly NOAA images. They have been assumed to exist in the KonTur area for ± 3 hours around the time of the satellite images.

Altogether, the footprints of cellular episodes in the large scale fields seem to be rather faint. The bulk of the derived quantitative data are near the limits of the used classical measurement capabilities.

Second, the calculation of divergences from the aerological data showed, that their values hardly ever surpassed the estimated accuracy limits. The major problem lies in the potentially very different fate of single radiosondes in heavily convective situations, in which their paths may lie near clouds or in the region of compensating subsidence. Due to strong and gusty winds not all of the scheduled sondes can really be launched, so that the evaluation of spacial gradients sometimes has to rely an interpolated data. The averaging and interpolation procedure itself may distribute extreme conditions, that happend to one sonde, to a longer time interval and to the total area. Nevertheless, after careful inspection of each single ascent the vertical and temporal homogeneity of the time series seems remarkable and trustworthy. On the other hand the calculation of gradients and, derived from these, of divergences seems to be at the accuracy limit of the available data.

Third, the derivation of a convective height is problematic as no striking inversion layers are found. The temperature profile is gradually transformed from unstable near the surface via nearly moist adiabatic in the cloud layer to stable above this. May be the best indicator of convection height is the relative humidity profile, that indicates rapid drying of the air above the cloud layer.

Acknowledgement

The authors wish to thank B. Busack and H. Koch for their support in data analysis, M. Grunert and M. Lüdicke for preparing the figures, and B. Zinecker for typing the manuscript.

References

Agee, E.M., T.S. Chen, K.E. Dowell (1973):
A review of mesoscale cellular convection. Bull. Americ. Meteorol. Soc., 54, 1004-1012

Bakan, S. (1985):
On the structure of open cellular convection as revealed by time series of surface observations: A case study. Beitr. Phys. Atmosph., 58, 11-16.

Becker, P. (1987):
Numerische Untersuchungen zur Dynamik zwei- und dreidimensionaler konvektiver Strukturen in einer durch eine Inversion abgeschlossenen atmosphärischen Grenzschicht. Hamb. Geophys. Einzelschr., 86, Hamburg.

Beniston, M. (1984):
A numerical study of mesoscale atmospheric cellular convection. Dyn. Atm. Oc., 8, 223-242.

Beniston, M. (1985):
Organization of convection in a numerical mesoscale model as a function of initial and lower boundary conditions. Beitr. Phys. Atmosph., 58, 31-52.

Brümmer, B. (1985):
Structure, dynamics and energetics of boundary layer rolls from KonTur aircraft observations. Beitr. Phys. Atmosph., 58, 237-254.

Brümmer, B., T. Fischer, S. Zank (1986):
Aircraft observations of open cellular structures during KonTur. Beitr. Phys. Atmosph., 59, 162-184..

Busack, B., S. Bakan, H. Luthardt (1985):
Surface conditions during mesoscale cellular convection. Beitr. Phys. Atmosph., 58, 4-10.

Chlond; A. (1985):
A study of roll vortices in the atmospheric boundary layer. Beitr. Phys. Atmosph., 58, 17-30.

Chlond, A. (1987):
A numerical study of horizontal roll vortices in neutral and unstable atmospheric boundary layers. Beitr. Phys. Atmosph., 60, 144-170.

Hinzpeter, H. (1985):
KonTur-Results. Beitr. Phys. Atmos., 58, 1-3.

Hoeber, H. (Ed., 1982):
KonTur - Field phase report. Hamb. Geophys. Einzelschr., Ser. B, Vol. I, Wittenborn Söhne, Hamburg.

Lenschow, D.H., E.M. Agee (1976):

Preliminary results from the air mass transformation experiment (AMTEX). Bull. American Meteor. Soc., 57, 1346-1355.

Luthardt, H. (1985):

Estimation of mesoscale surface fields of meteorological parameters in the North Sea area from routine observations. Beitr. Phys. Atmos., 58, 255-272.

Krueger, A.F., S. Fritz (1961):

Cellular cloud patterns revealed by TIROS I. Tellus, 13, 1-7.

Sheu, P.J., E.M. Agee (1977):

Kinematic analysis and air-sea heat flux associated with mesoscale cellular convection during AMTEX 1975. J. Atmos. Sci., 34, 793-801.

Shirer, H.N. (1986):

On cloud street development in three dimensions: Parallel and Rayleigh instabilities. Beitr. Phys. Atmosph., 59, 126-149.

Shirer, H.N., B. Brümmer (1986):

Cloud streets during KonTur: A comparison of parallel/thermal instability modes with observations. Beitr. Phys. Atmos., 59, 150-161.

	PHASE I	PHASE II	TOTAL
Planned launches:	103 (= 100%)	75 (= 100%)	178 (= 100%)

Number of complete soundings/failures in % of planned soundings:

	PHASE I	PHASE II	TOTAL
METEOR	98 / 5	67 / 11	165 / 7
GAUSS/POSEIDON	85 / 17	60 / 20	145 / 22
ELBE 1	80 / 22	58 / 23	138 / 22
BORKUM RIFF	90 / 13	54 / 28	144 / 19

Simultaneous soundings at "N" stations/in % of planned soundings:

	PHASE I	PHASE II	TOTAL
N = 2	97 / 94	71 / 95	168 / 94
N ≥ 3	88 / 85	55 / 73	143 / 80
N = 4	63 / 61	38 / 51	101 / 57

Table 1: Data volume of aerological data set gained during KonTur 1981.

		Preceeding phase A			Cellular phase B			Succeeding phase C		
Surface	ΔT [K]	-4.5°			-5.2°			-5.0°		°C
	Δq [g/kg]	-4.4			-4.8			-4.8		g/kg
	FF [m/s]	14.3			10.2			6.5		m/s
	H [W/m²]	113			93			55		W/m²
	B	0.43			0.53			0.52		
		T[K]	|v| [m/s]	p[hPa]	T[K]	|v| [m/s]	p[hPa]	T[K]	|v| [m/s]	p[hPa]
Tendencies per 3 h	10 m	-0.9	1.1	1.8	0.0	-0.8	0.0	0.5	-0.9	0.0
	1000 m	-1.2	0.7	2.4	0.0	-1.4	0.0	0.5	-1.9	0.0
	3000 m	-1.4	0.5	0.9	0.0	-1.1	0.2	0.7	-2.8	0.6
	4500 m	-1.6	-0.6	0.6	0.5	0.4	0.5	1.2	-1.3	0.6
Advection - v grad T]°C/day]	10 m	-8			-3			3		
	1000 m	-6			0			8		
	3000 m	-12			0			15		
	4500 m	-10			5			20		
div. v [10^5 s^{-1}]	10 m	-1.5			-0.5			0.0		
	1000 m	-2.0			0.0			-0.5		
	3000 m	-1.5			-0.5			-1.5		
	4500 m	-0.5			-2.0			-2.0		

Table 2: Selected data during preceeding and succeeding a phase of well expressed cellular activity on Oct. 14, 1981 (v - wind vector, T - temperature, q - specific humidity, p - pressure, H - sensible heat, B - Bowen ratio, Δ indicates air-sea difference).

Figure 1a: Open cellular convection over the North Sea during the experiment KonTur 1981 (LANDSAT II, Oct. 15, 1981, 1000 LT, area size 185 x 185 km²).

Figure 1b: Schematic of open cellular secondary circulation.

Figure 2: The network of aerological stations (C - Center of the experiment area, FPN - Forschungsplattform Nordsee) and their mutual distance in km.

Figure 3: Height coverage of the launched radiosondes at the various platforms during the second phase of KonTur in October 1981.

Figure 4: 850 hPa height and temperature contours for the North-Eastern Atlantic at 00 UT between October 9 and 16, 1981 (from the "Berliner Wetterkarte").

Figure 5: Horizontally averaged surface data and synoptic events:
P_{NN}: pressure at NN. T_W: water bucket temperature. T_A: air temperature in 10 m height. RF: relative humidity. DD: wind direction. FF: wind speed. H = sensible heat, lE = latent heat, B = bowen ratio, z/L = Monin-Obukhov stability, LCL = lifting condensation level.
Air mass characterization: mn: maritim, A: arctic, P: polar, S: steered over subtropic regions.
Hatched areas indicate occurrence of organized convection.

Figure 6: Time height cross-section of potential temperature (Θ in K).

Figure 7: Time height cross-section of specific humidity (q in g/kg).

Figure 8: Time height cross-section of relative humidity (RH in %)

Figure 9: Time height cross-section of equipotential temperature (Θ_e in K).

Figure 10: Time height cross-section of wind speed ($|V|$ in m/s).

Figure 11: Pressure gradient field. Arrows direct into deep pressure center. Calibration arrow on the right side in hPa /1000 km points toward north.

Figure 12: Mean spatial temperature gradient vector field (baroclinicity). Arrows direct into cold center. Calibration arrow on the right side in (K/1000 km).

Figure 13: Time height cross-section of temperature advection.

Figure 14: Mean spacial humidity gradient vector field. Arrows direct into dry center. Calibration arrow on the right side in (g/kg)/1000 km.

Figure 15: Time height cross-section of divergence.

Figure 16: Mean vertical structure of several quantities before (A), during (B) and after (C) the best expressed cellular episode (Θ_w - water bucket temperature, Θ_{ew} - water equipotential temperature).

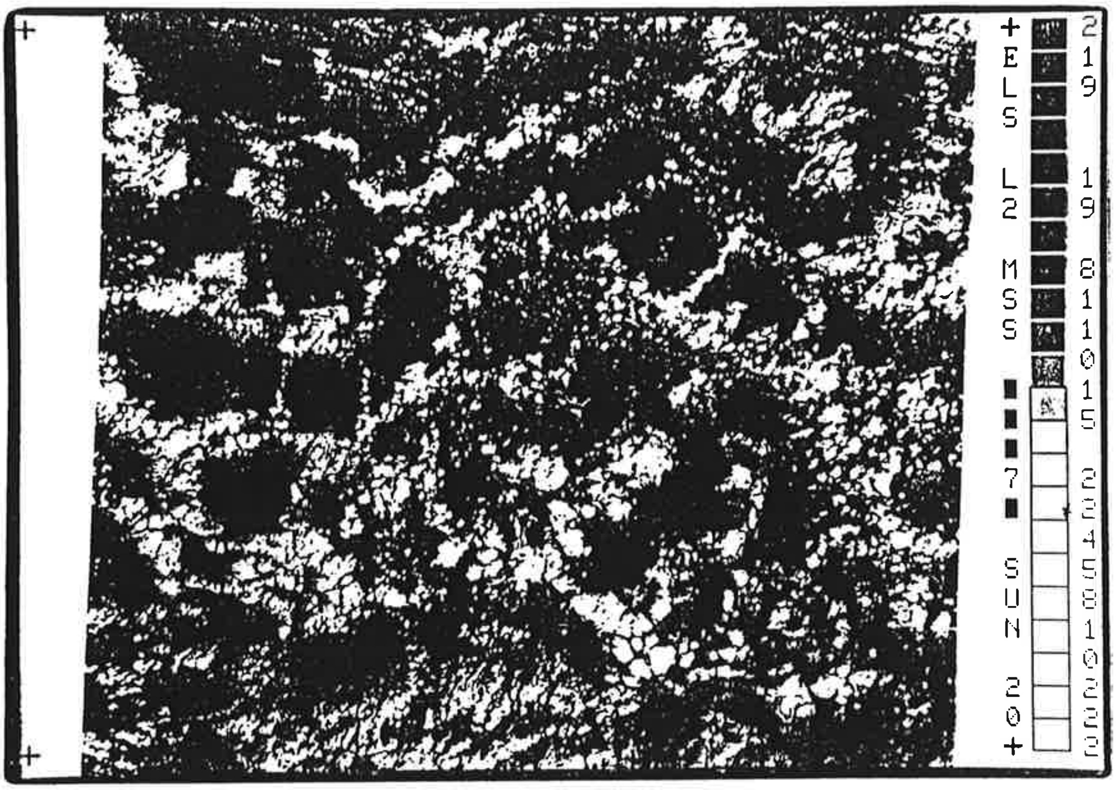

FIG. 1a

OPEN CONVECTION CELLS

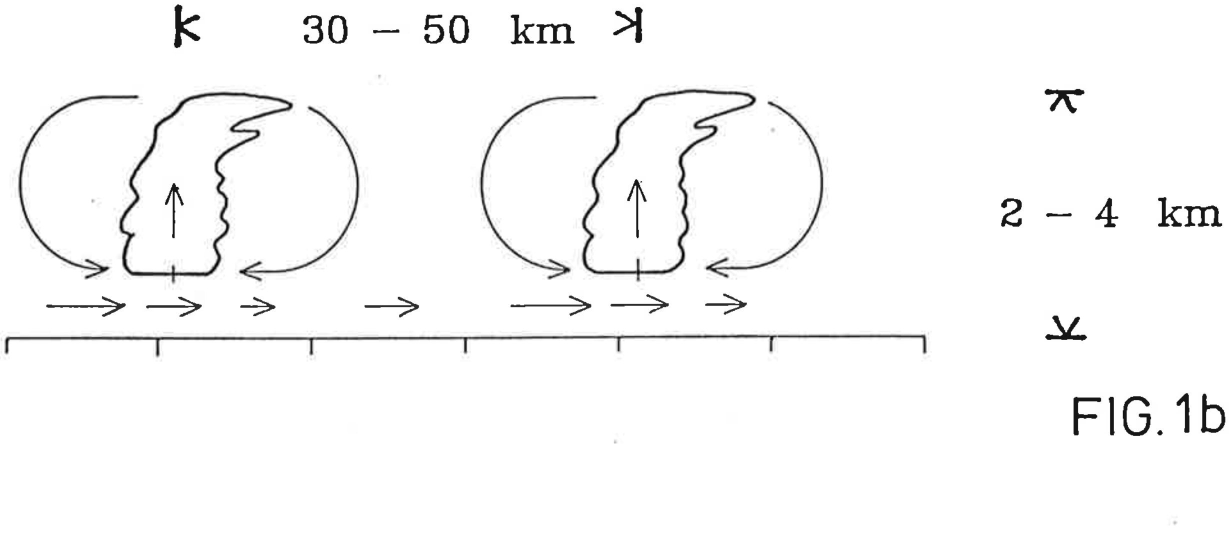

FIG. 1b

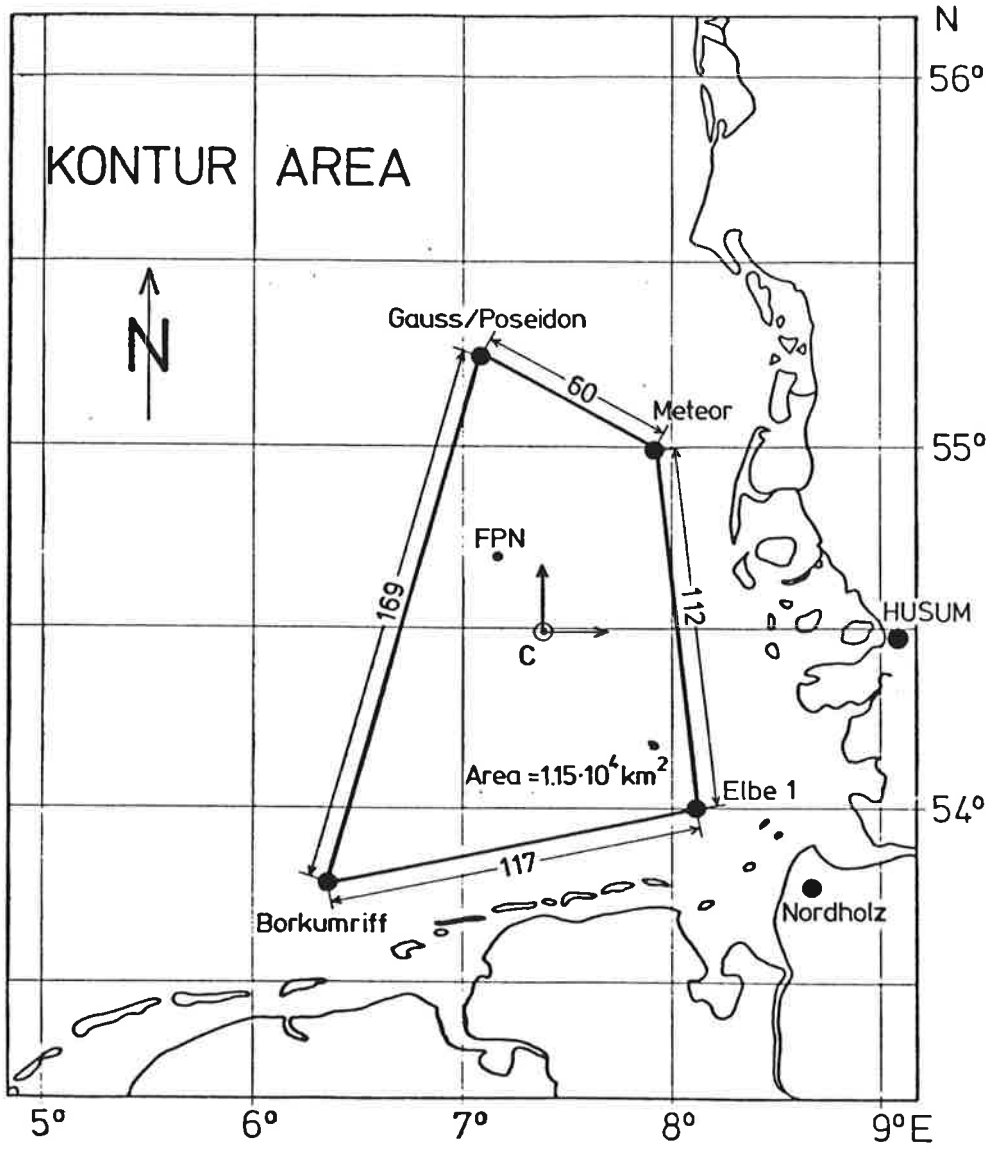
KONTUR AREA
N
Gauss/Poseidon
60
Meteor
FPN
C
169
112
HUSUM
Area =1.15·10⁴km²
Elbe 1
117
Borkumriff
Nordholz
N
56°
55°
54°
5°
6°
7°
8°
9°E

FIG. 2

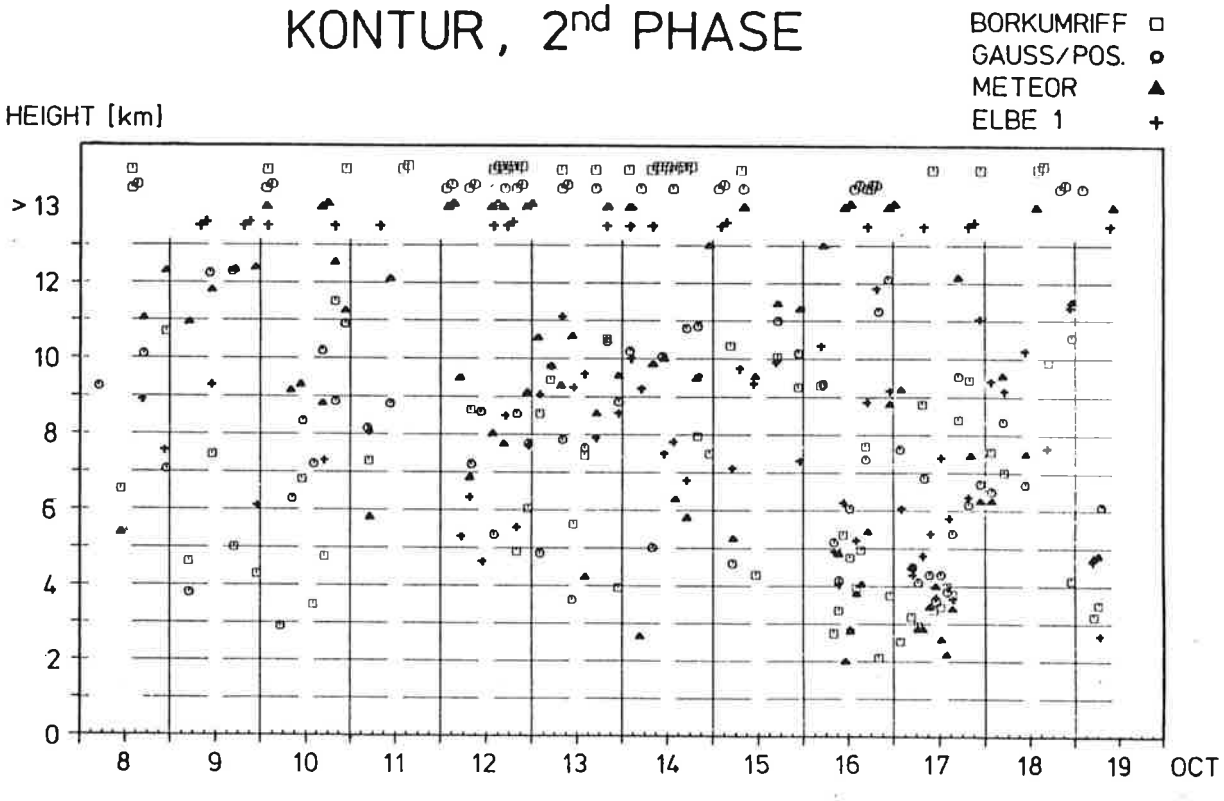
KONTUR, 2nd PHASE
BORKUMRIFF
GAUSS/POS.
METEOR
ELBE 1
HEIGHT [km]
> 13
12
10
8
6
4
2
0
8
9
10
11
12
13
14
15
16
17
18
19
OCT

FIG. 3

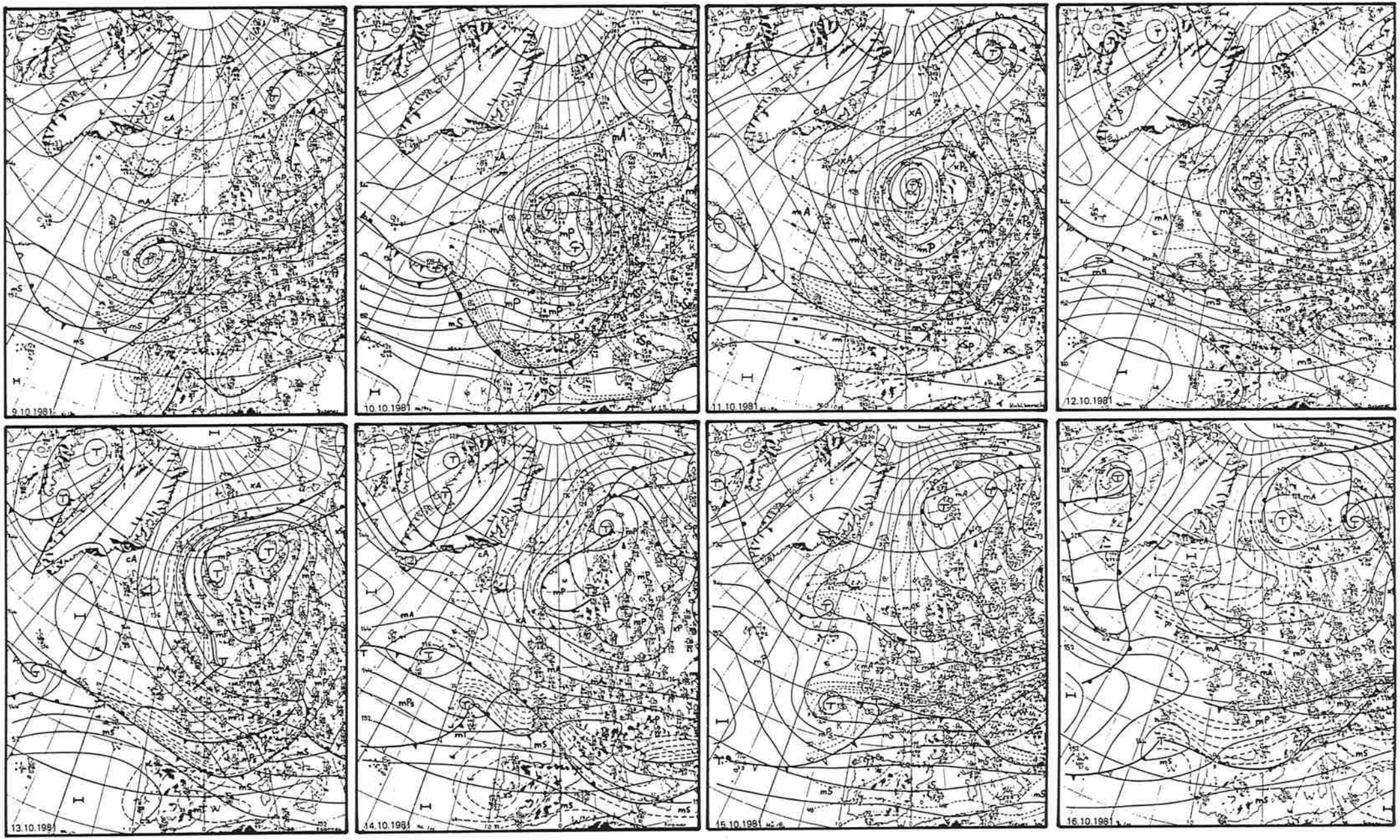
9.10.1981
10.10.1981
11.10.1981
12.10.1981
13.10.1981
14.10.1981
15.10.1981
16.10.1981

FIG. 4

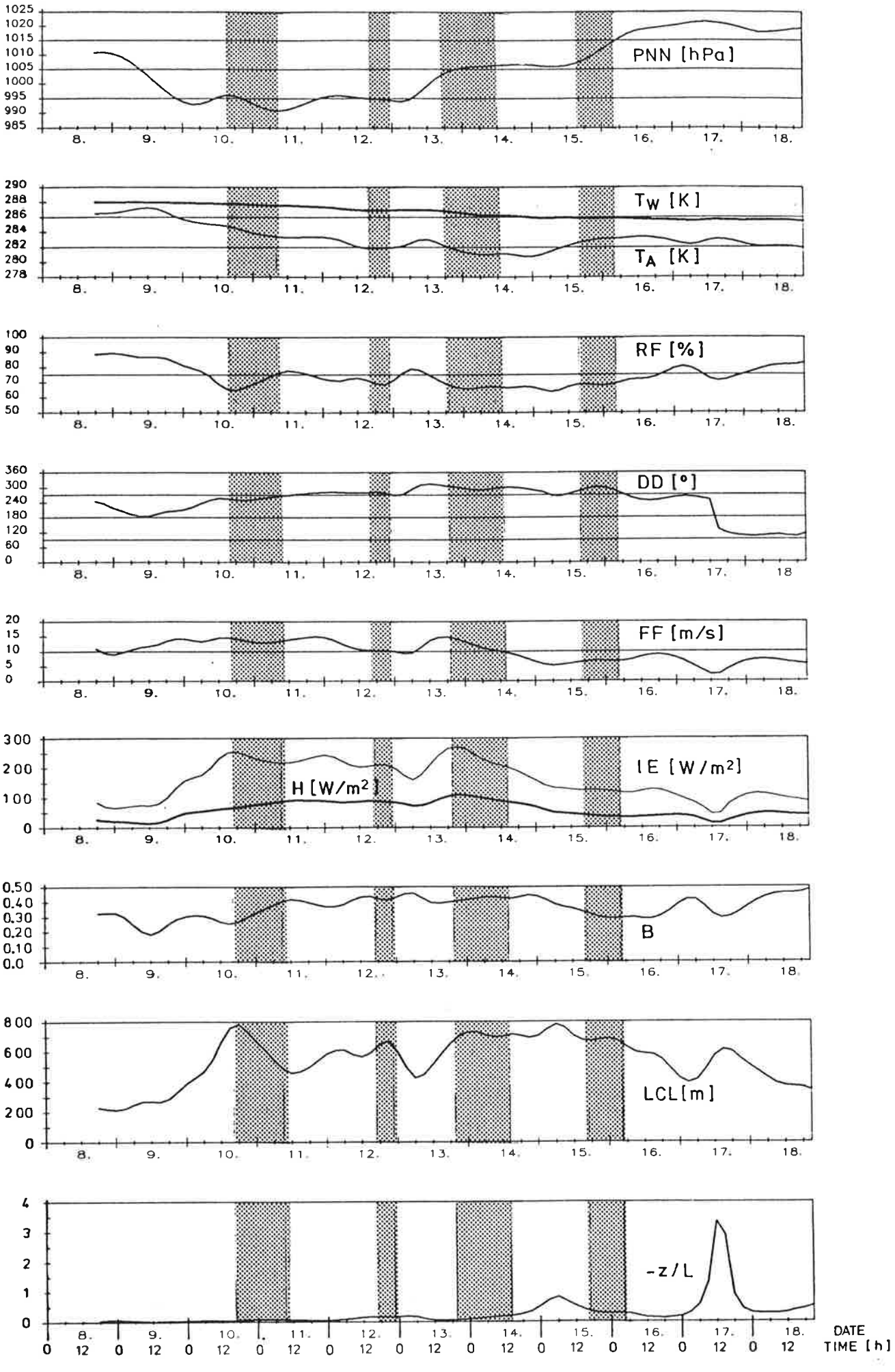
PNN [hPa]
1025
1020
1015
1010
1005
1000
995
990
985
T_W [K]
T_A [K]
290
288
286
284
282
280
278
RF [%]
100
90
80
70
60
50
DD [°]
360
300
240
180
120
60
0
FF [m/s]
20
15
10
5
0
H [W/m²]
IE [W/m²]
300
200
100
0
B
0.50
0.40
0.30
0.20
0.10
0.0
LCL [m]
800
600
400
200
0
-z/L
4
3
2
1
0
8. 9. 10. 11. 12. 13. 14. 15. 16. 17. 18.
0 12 0 12 0 12 0 12 0 12 0 12 0 12 0 12 0 12 0 12 0 12
DATE
TIME [h]

FIG. 5

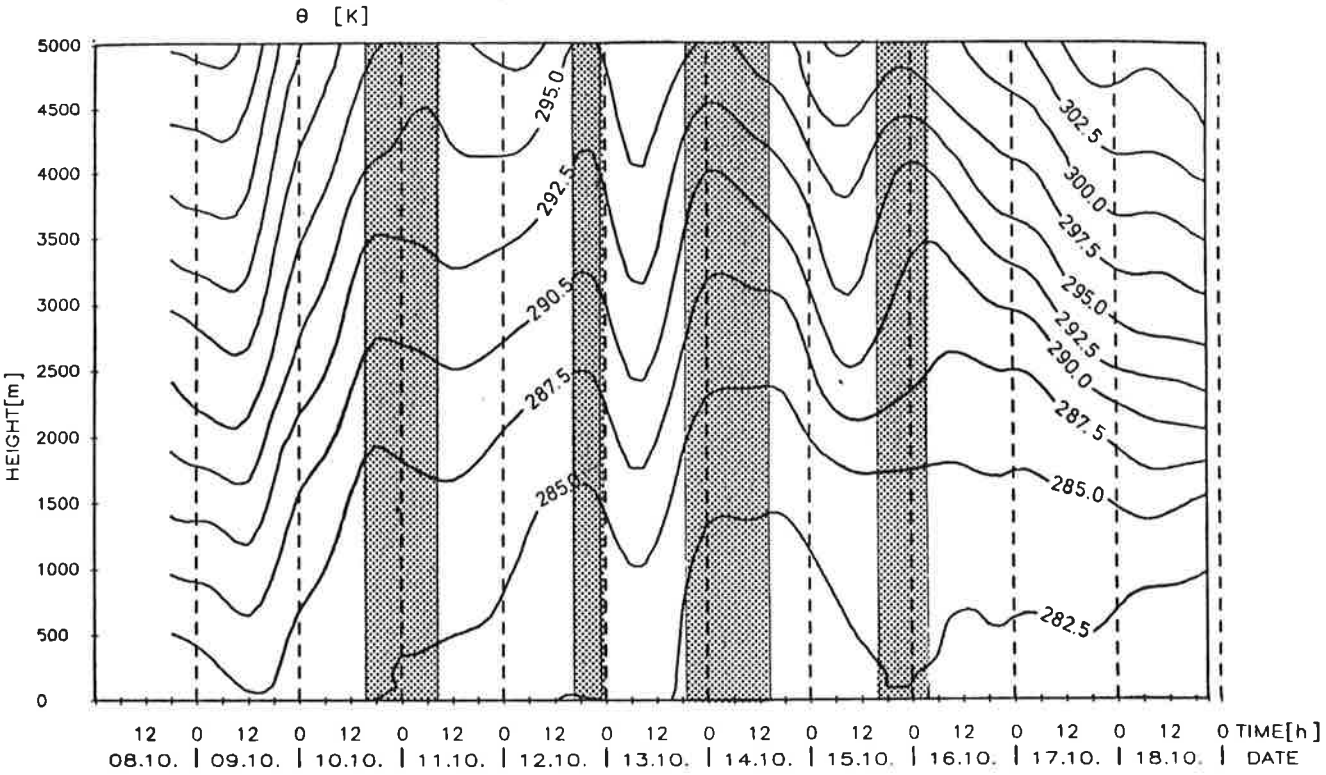
θ [K]
HEIGHT[m]
5000
4500
4000
3500
3000
2500
2000
1500
1000
500
0
295.0
292.5
290.5
287.5
285.0
302.5
300.0
297.5
295.0
292.5
290.0
287.5
285.0
282.5
12 0 12 0 12 0 12 0 12 0 12 0 12 0 12 0 12 0 12 0 12 0 TIME[h]
08.10. 09.10. 10.10. 11.10. 12.10. 13.10. 14.10. 15.10. 16.10. 17.10. 18.10. DATE

FIG. 6

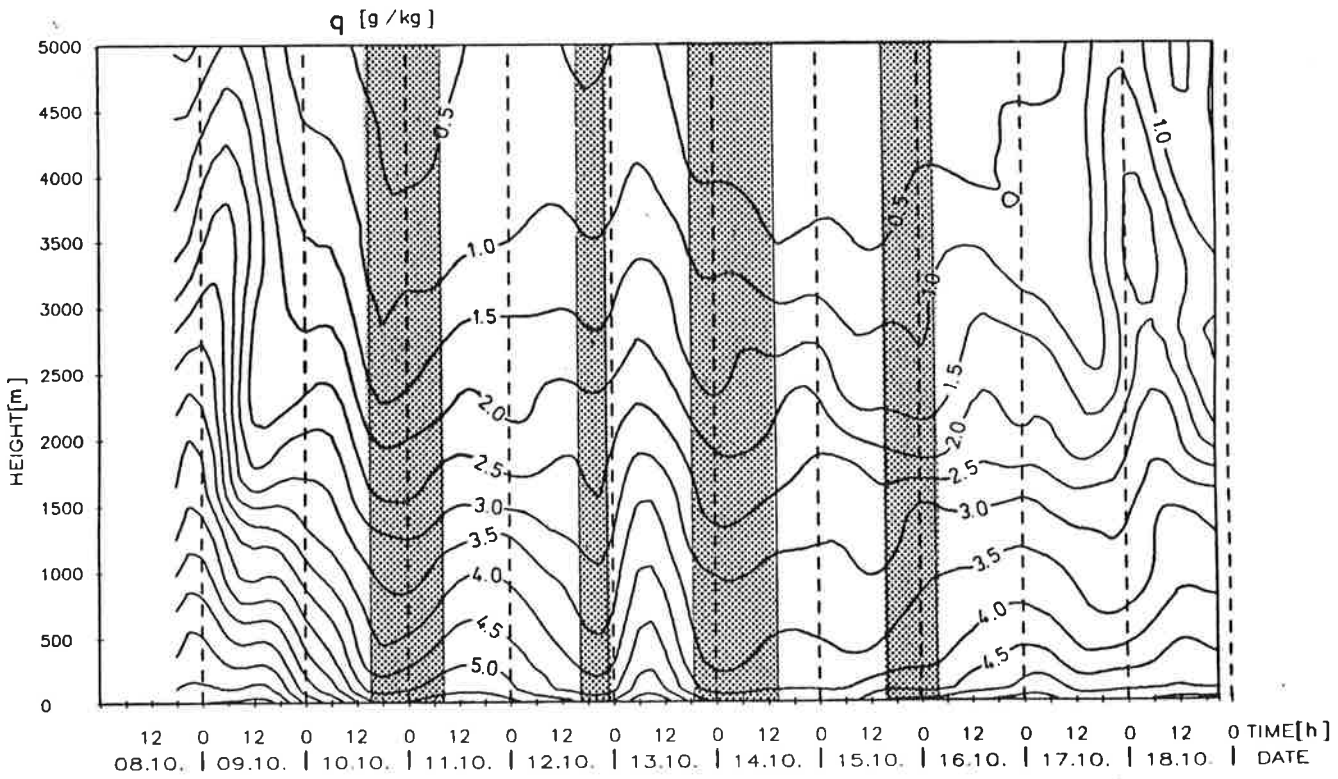
q [g/kg]
HEIGHT[m]
5000
4500
4000
3500
3000
2500
2000
1500
1000
500
0
0.5
1.0
1.5
2.0
2.5
3.0
3.5
4.0
4.5
5.0
0
0.5
1.0
1.5
2.0
2.5
3.0
3.5
4.0
4.5
12 0 12 0 12 0 12 0 12 0 12 0 12 0 12 0 12 0 12 0 12 0 TIME[h]
08.10. 09.10. 10.10. 11.10. 12.10. 13.10. 14.10. 15.10. 16.10. 17.10. 18.10. DATE

FIG. 7

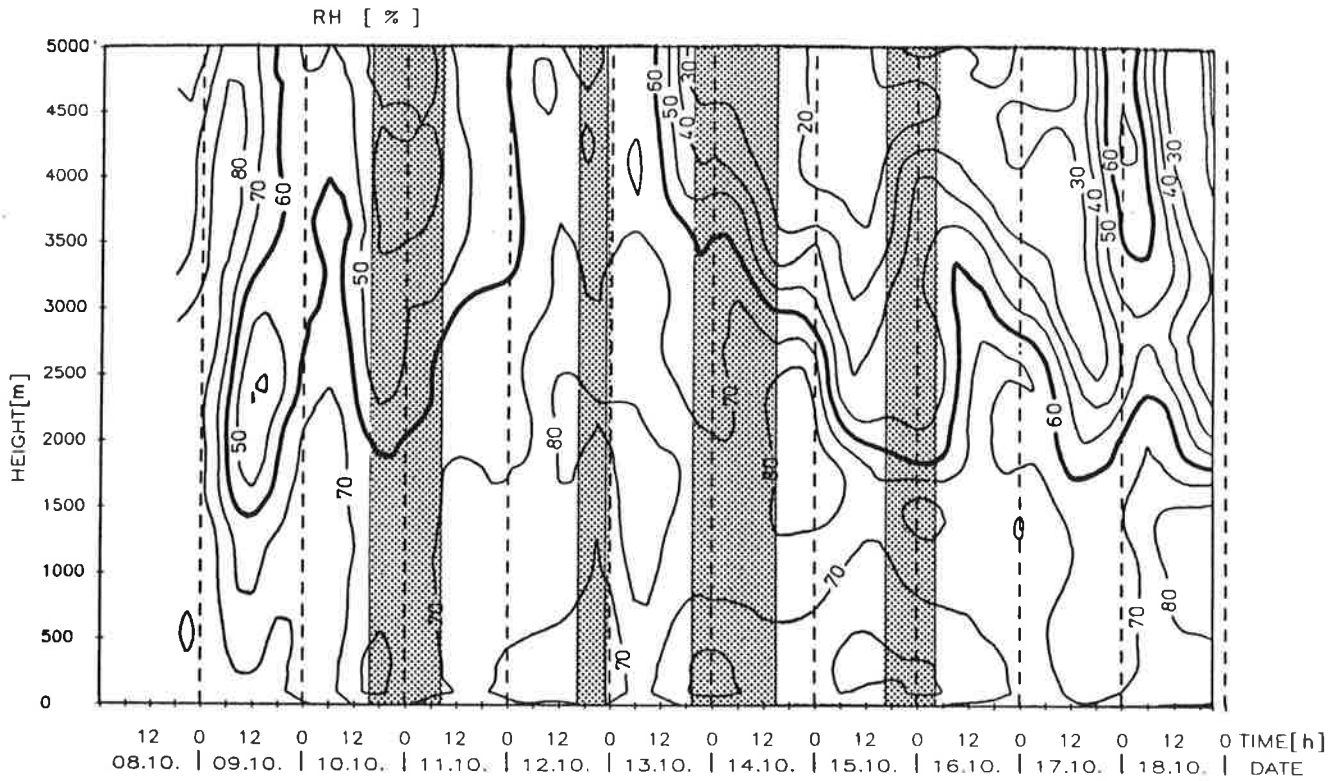
RH [%]
HEIGHT[m]
5000
4500
4000
3500
3000
2500
2000
1500
1000
500
0
12 0 12 0 12 0 12 0 12 0 12 0 12 0 12 0 12 0 12 0 12 0 TIME[h]
08.10. 09.10. 10.10. 11.10. 12.10. 13.10. 14.10. 15.10. 16.10. 17.10. 18.10. DATE

FIG. 8

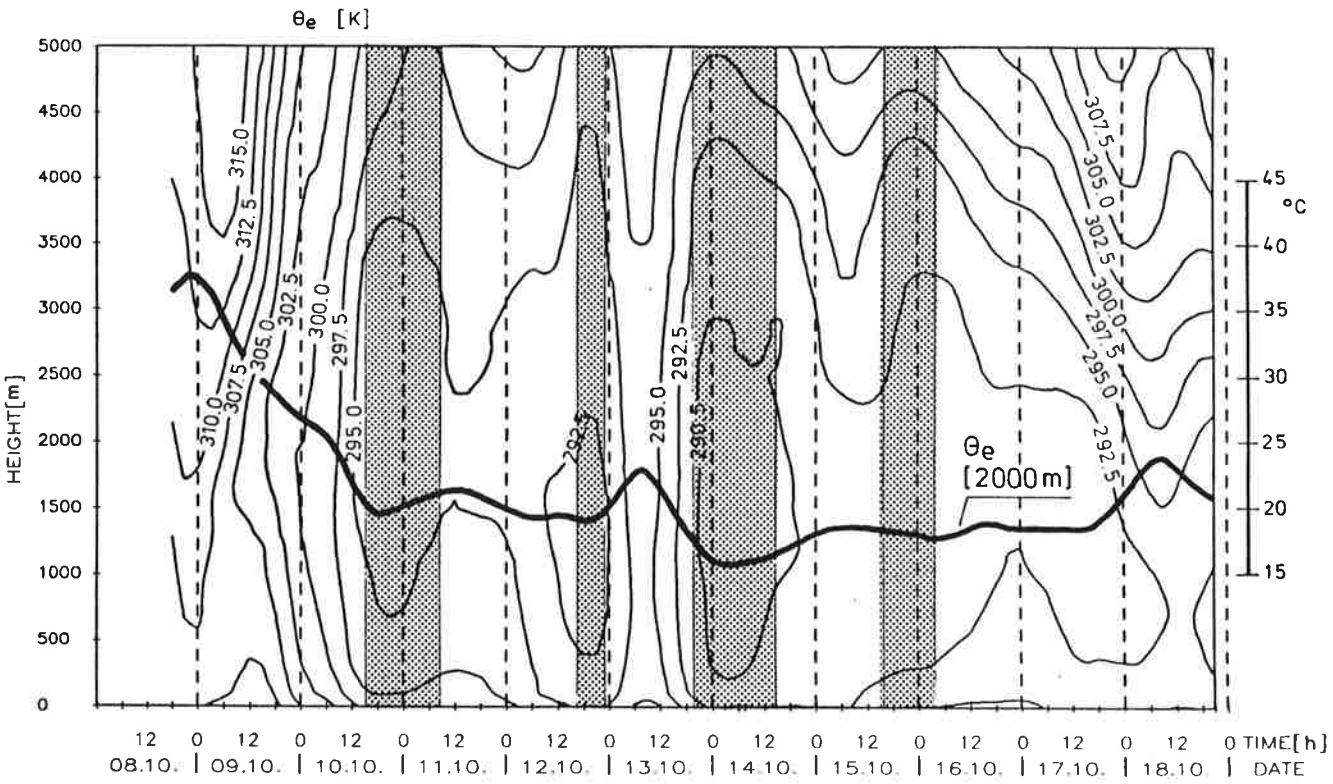
θe [K]
HEIGHT[m]
5000
4500
4000
3500
3000
2500
2000
1500
1000
500
0
θe
[2000m]
45
°C
40
35
30
25
20
15
12 0 12 0 12 0 12 0 12 0 12 0 12 0 12 0 12 0 12 0 12 0 TIME[h]
08.10. 09.10. 10.10. 11.10. 12.10. 13.10. 14.10. 15.10. 16.10. 17.10. 18.10 DATE

FIG. 9

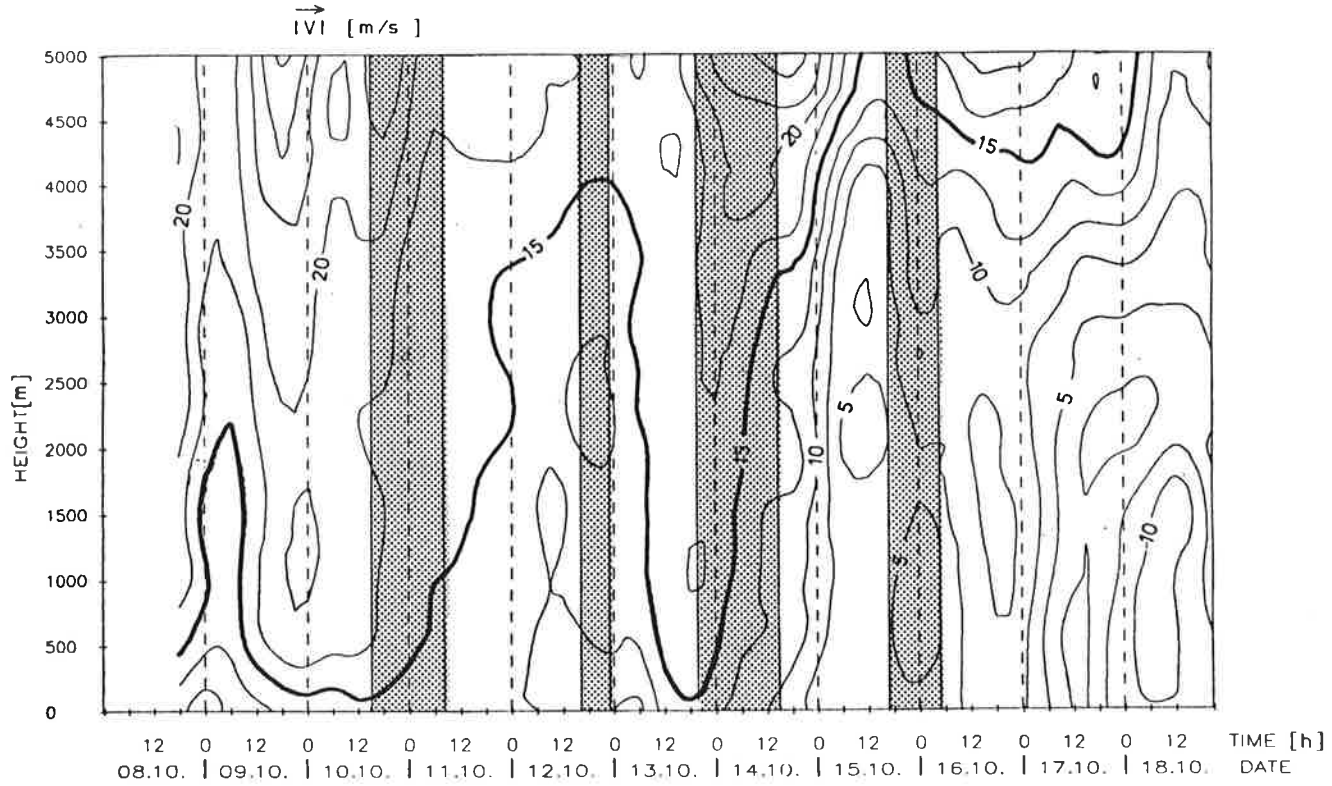
|v| [m/s]
HEIGHT[m]
5000
4500
4000
3500
3000
2500
2000
1500
1000
500
0
20
15
10
5
12 0 12 0 12 0 12 0 12 0 12 0 12 0 12 0 12 0 12 0 12
TIME [h]
08.10. 09.10. 10.10. 11.10. 12.10. 13.10. 14.10. 15.10. 16.10. 17.10. 18.10.
DATE

FIG. 10

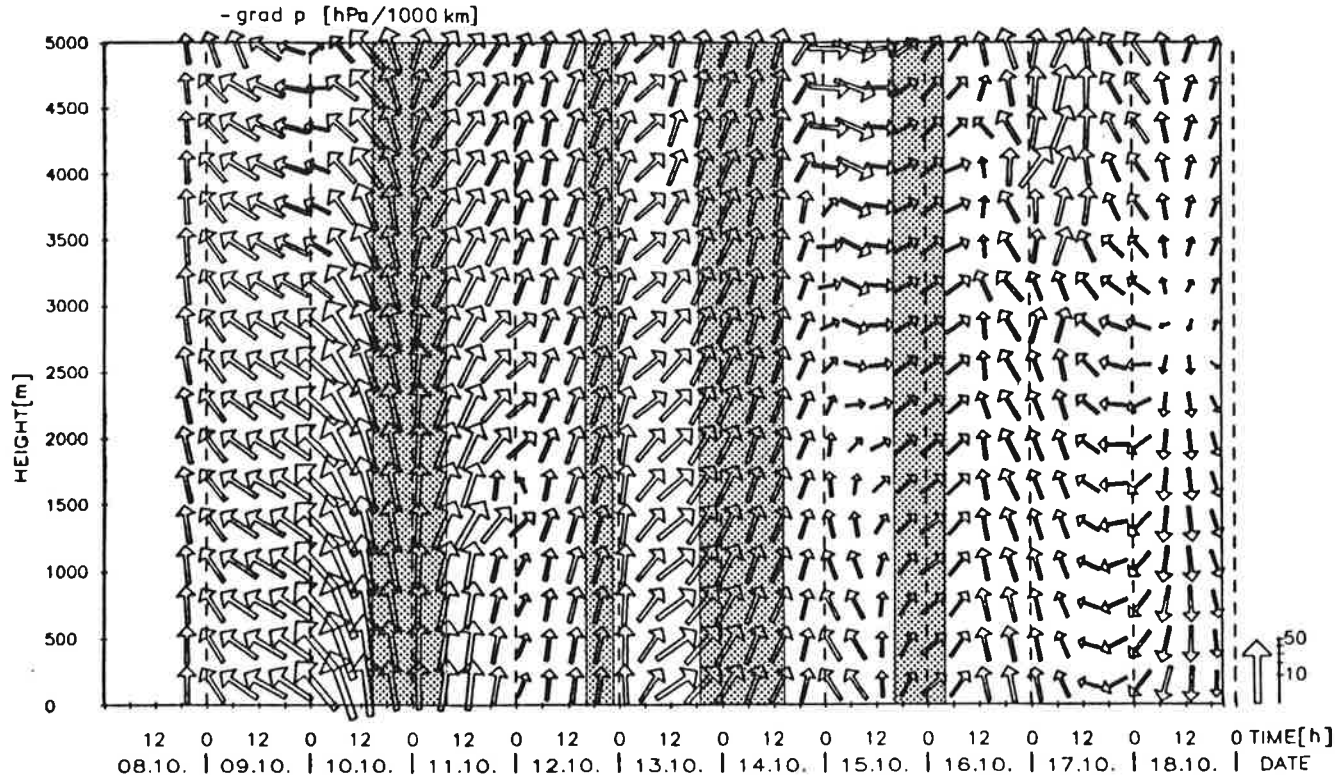
- grad p [hPa/1000 km]
HEIGHT[m]
5000
4500
4000
3500
3000
2500
2000
1500
1000
500
0
50
10
12 0 12 0 12 0 12 0 12 0 12 0 12 0 12 0 12 0 12 0 12 0
TIME[h]
08.10. 09.10. 10.10. 11.10. 12.10. 13.10. 14.10. 15.10. 16.10. 17.10. 18.10.
DATE

FIG. 11

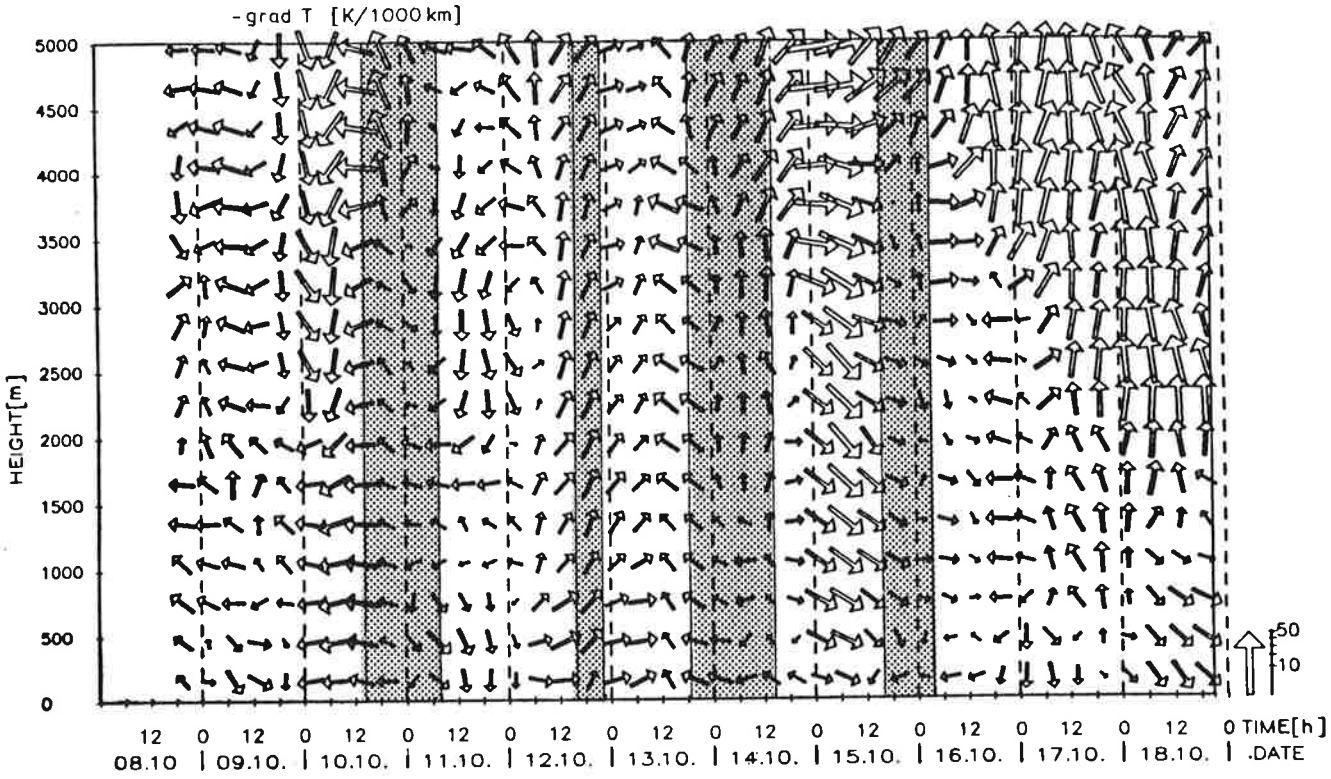

FIG. 12

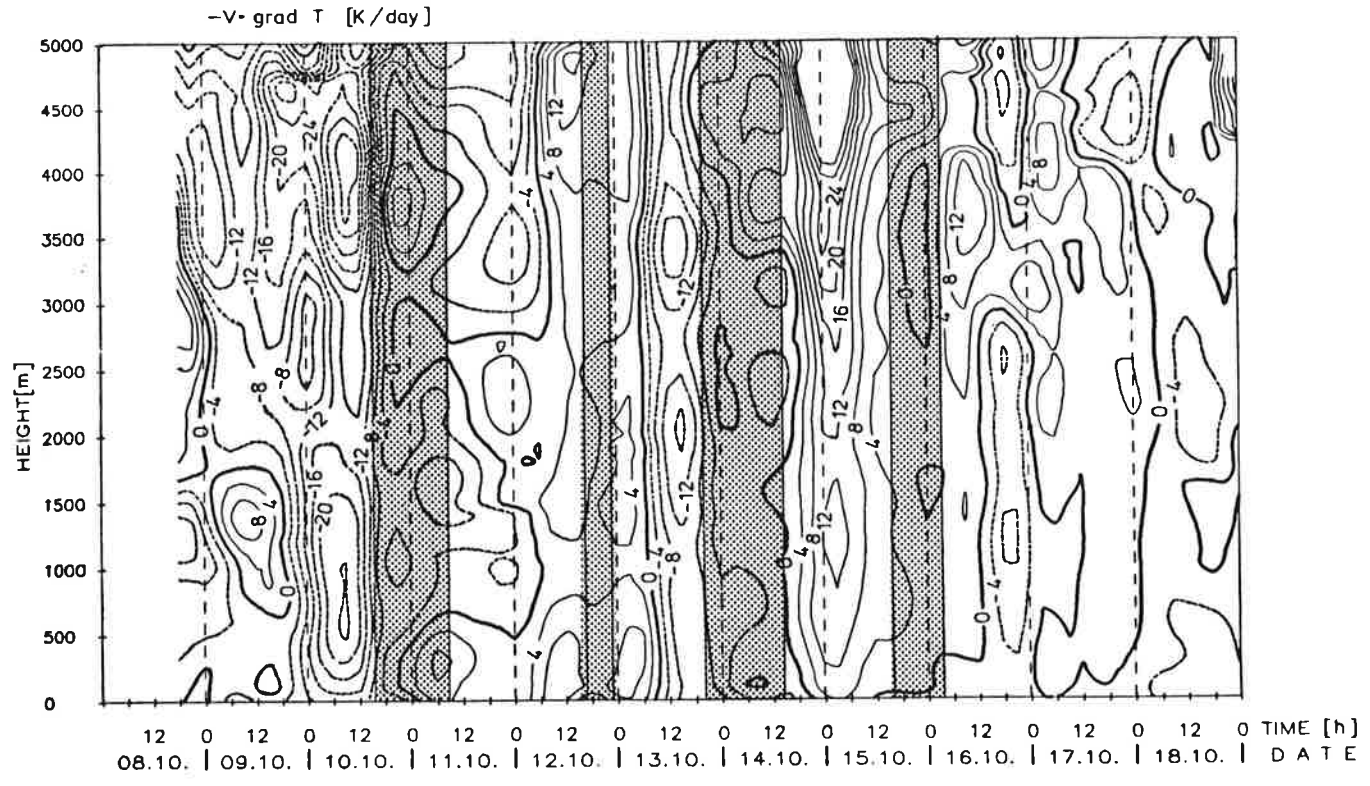

FIG. 13

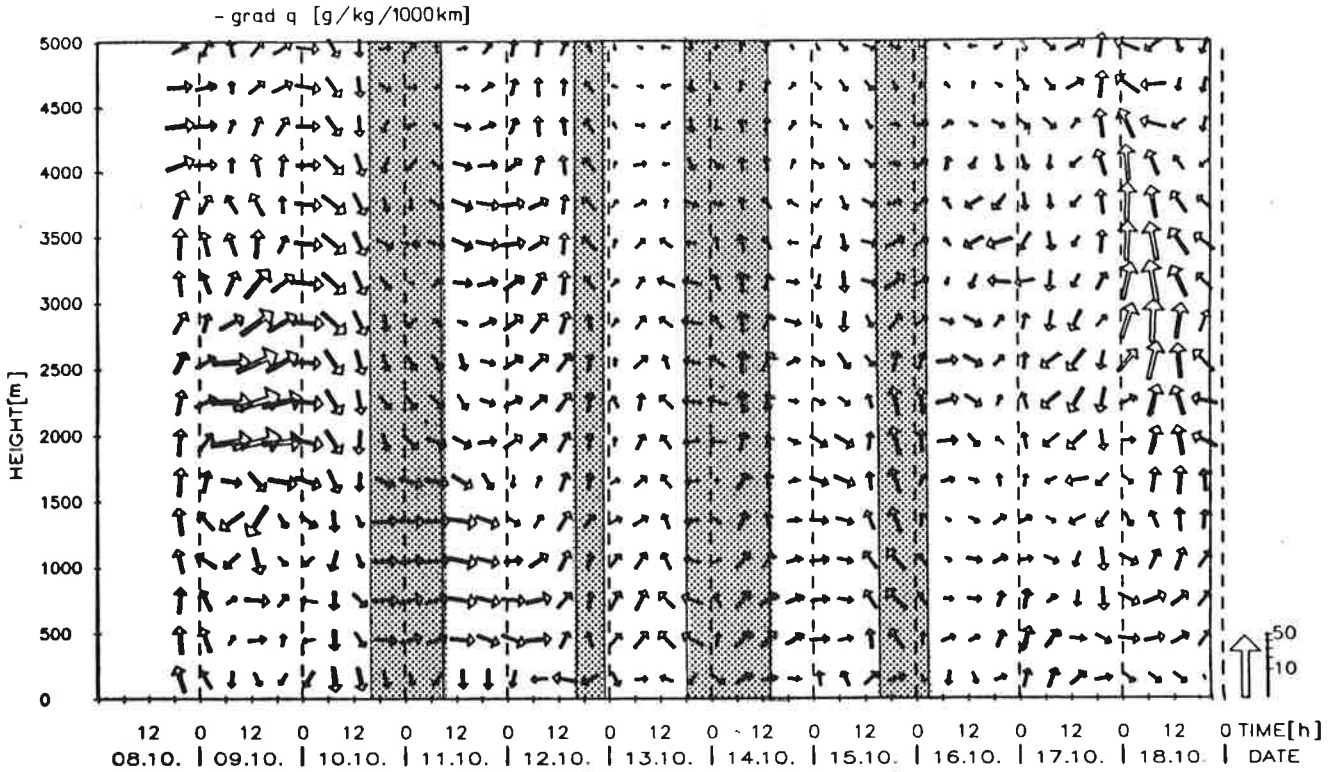
- grad q [g/kg/1000km]
HEIGHT[m]
5000
4500
4000
3500
3000
2500
2000
1500
1000
500
0
50
10
12 0 12 0 12 0 12 0 12 0 12 0 12 0 12 0 12 0 12 0 12 0 TIME[h]
08.10. 09.10. 10.10. 11.10. 12.10. 13.10. 14.10. 15.10. 16.10. 17.10. 18.10. DATE

FIG. 14

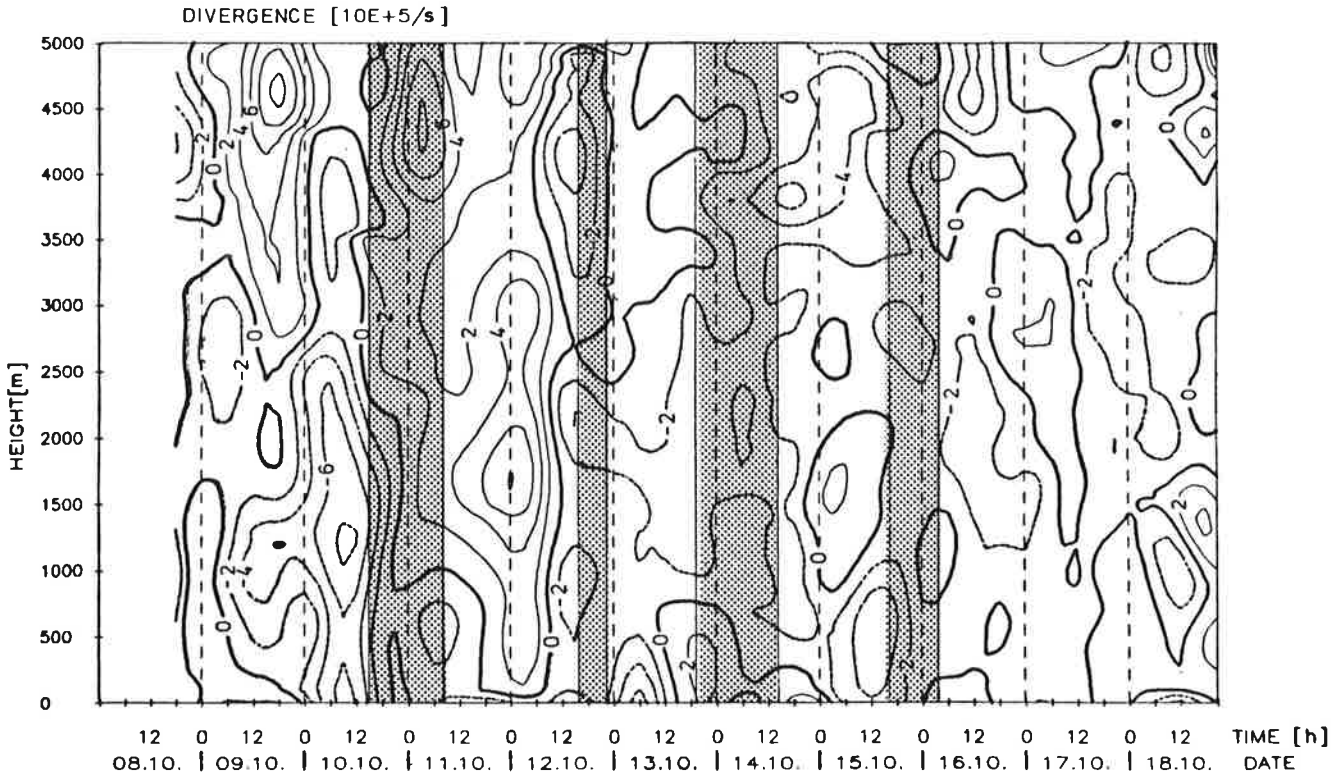
DIVERGENCE [10E+5/s]
HEIGHT[m]
5000
4500
4000
3500
3000
2500
2000
1500
1000
500
0
12 0 12 0 12 0 12 0 12 0 12 0 12 0 12 0 12 0 12 0 12 0 TIME [h]
08.10. 09.10. 10.10. 11.10. 12.10. 13.10. 14.10. 15.10. 16.10. 17.10. 18.10. DATE

FIG. 15

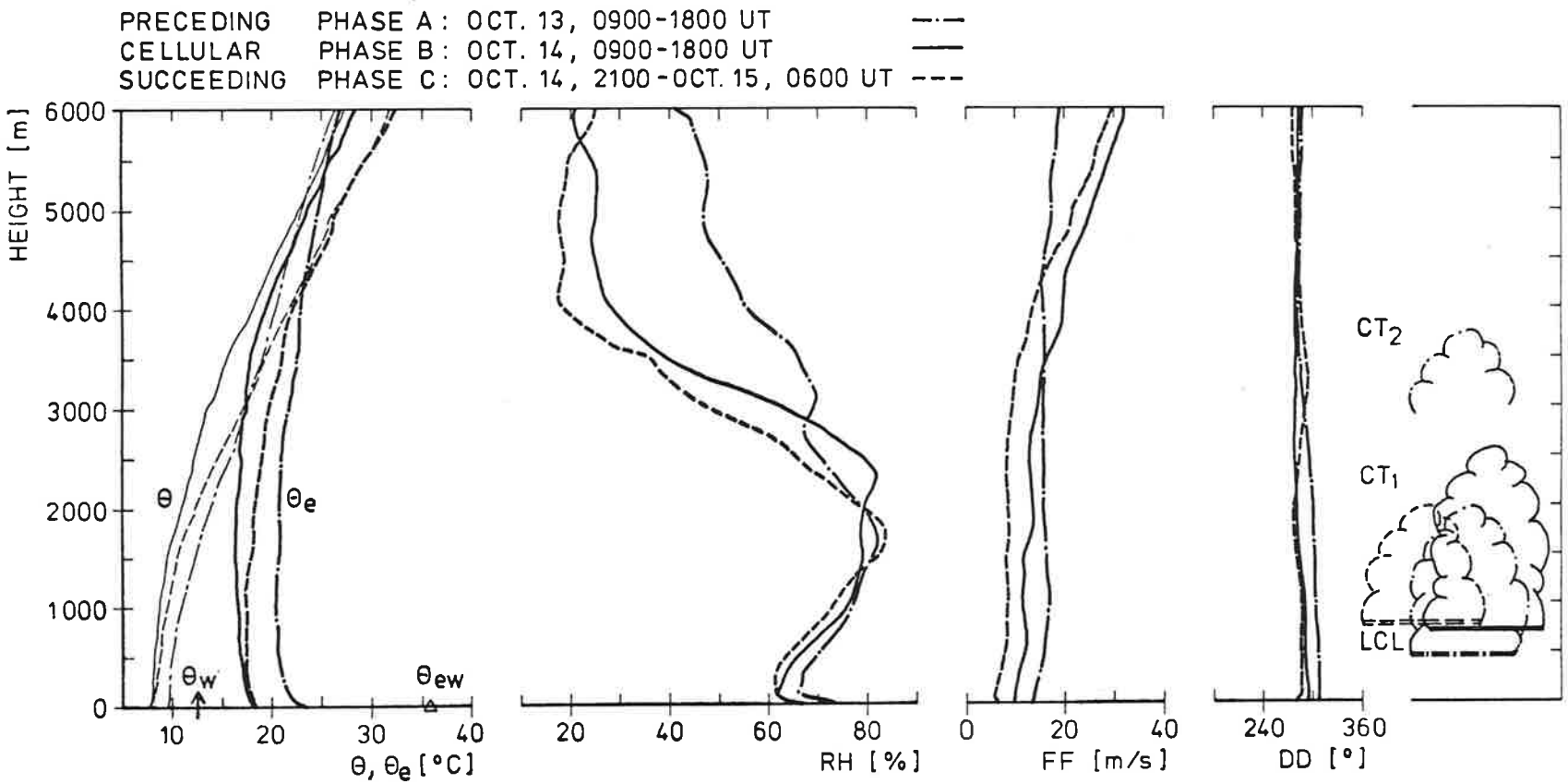
PRECEDING PHASE A: OCT. 13, 0900-1800 UT
CELLULAR PHASE B: OCT. 14, 0900-1800 UT
SUCCEEDING PHASE C: OCT. 14, 2100-OCT. 15, 0600 UT
HEIGHT [m]
6000
5000
4000
3000
2000
1000
0
θ
θe
θw
θew
10
20
30
40
θ, θe [°C]
20
40
60
80
RH [%]
0
20
40
FF [m/s]
240
360
DD [°]
CT2
CT1
LCL

FIG. 16